Conformational Preferences and Vibrational Frequency Distributions of Short Peptides in Relation to Multidimensional Infrared Spectroscopy

S. Gnanakaran and R. M. Hochstrasser*

Contribution from the University of Pennsylvania, Philadelphia, Pennsylvania 19104-6323

Received April 30, 2001

Abstract: Molecular dynamics simulations of the structural distributions and the associated amide-I vibrational modes are carried out for dialanine peptide in water and carbon tetrachloride. The various manifestations in nonlinear-infrared spectroscopic experiments of the distributions of conformations of solvated dialanine are examined. The two-dimensional infrared (2D-IR) spectrum of dialanine exhibits the coupling between the amide oscillators and the correlations of the frequency fluctuations. An internally hydrogen-bonded conformation exists in CCl_4 but not in H_2O where two externally hydrogen-bonded forms are preferred. Simulations of solvated dialanine show how the 2D-IR spectra expose the underlying structural distributions and dynamics that are not deducible from linear-infrared spectra. In H_2O the 2D-IR shows cross-peaks from large coupling in the α-helical conformer and an elongated higher frequency diagonal peak, reflecting the broader distribution of structures for the more flexible acetyl end. In CCl_4, the computed cross-peak portion of the 2D-IR shows evidence of two amide-I transitions in the high-frequency region which are not apparent from the diagonal peak profile. The vibrational frequency inhomogeneity of the amide-I band arises from fluctuations of the instantaneous normal modes of these conformers rather than the shifts induced by hydrogen bonding. The simulation shows that there are correlations between fluctuations of the acetyl and amino end frequencies in H_2O that arise from mechanical coupling and not from hydrogen bonding at the two ends of the molecule. The angular relationships between the two amide units which also show up in 2D-IR were computed, and spectral manifestations of them are discussed. The simulations also permit a calculation of the rate of energy transfer from one side of the molecule to the other. From these calculations, 2D-IR spectroscopy in conjunction with simulations is seen to be a promising tool for determining dynamics of structure changes in dipeptides.

Introduction

Linear-infrared spectroscopy provides a fingerprint of various nuclear motions in a molecule. In proteins, motions of each peptide unit give rise to nine characteristic vibrational frequencies. Out of these, the amide-I band has been used extensively in structure studies because of its sensitivity to the secondary structure of proteins.[1,2] The alpha-helical structure gives rise to a single amide-I band typically in the region of 1650 cm^{-1}, whereas beta sheet give rises to two bands: a strong one at 1620 cm^{-1} and a weak one at 1690 cm^{-1}.[3] According to normal mode calculations, most of the contribution to the amide-I band is from the C═O stretch. The sensitivity of the amide-I band to the structure is due mainly to two effects; the frequency shift from external/internal hydrogen bonding of C═O; and the vibrational transition moment interaction of neighboring units.[2] Utilization of linear-infrared spectra (IR) to deduce three-dimensional structures of proteins and peptides has been limited because of the congestion from overlapping amide-I bands associated with different structural domains. Another challenge is to differentiate between the band structures that arise due to the vibrational excitonic interactions and those energy shifts from environmental fluctuations.

Experimental methodologies based on nonlinear-IR spectroscopy can overcome many of those shortcomings and lead us toward providing structural information. Such a promise has led to technological advances on developing multidimensional IR spectroscopy. Until recently, multidimensionality in the IR spectrum has been achieved by using temperature or pressure as an additional dimension.[4] However, recent developments in laser spectroscopy have led to novel two-dimensional infrared (2D-IR) experiments where the multidimensionality is achieved by several successive interactions between the field and the system.[5−8] In magnetic resonance, for example, the disentangling of complex spectra is accomplished by multiple pulse sequences that manipulate the spin coherences and populations.[9,10] An analogous approach in infrared spectroscopy requires the sample to be examined by multiple IR pulses having well-defined spectral bandwidth, phase, and amplitude.[11,12] From such

(1) Krimm, S.; Bandekar, J. *Adv. Protein Chem.* **1986**, *38*, 181−364.
(2) Tori, H.; Tasumi, M. *J. Chem. Phys.* **1992**, *96*, 3379−3387.
(3) Mantsch, H.; Chapman, D., Eds. *Infrared Spectroscopy of Biomolecules*; Wiley: New York, 1996.
(4) Noda, I. *App. Spectrosc.* **1990**, *44*, 550−561.
(5) Zanni, M. T.; Asplund, M. C.; Hochstrasser, R. M. *J. Chem. Phys.* **2001**, *114*, 4579−4590.
(6) Asplund, M. C.; Zanni, M. T.; Hochstrasser, R. M. *Proc. Natl. Acad. Sci. U.S.A.* **2000**, *97*, 8219−8224.
(7) Hamm, P.; Lim, M.; DeGrado, W. F.; Hochstrasser, R. M. *Proc. Natl. Acad. Sci. U.S.A.* **1999**, *96*, 2036−2041.
(8) Hamm, P.; Lim, M.; Hochstrasser, R. M. *J. Phys. Chem. B* **1998**, *102*, 6123−6138.
(9) Ernst, R. R.; Bodenhausen, G.; Wokaun, A. *Principles of Nuclear Magnetic Resonance in One and Two Dimensions*; Oxford University Press: Oxford, UK, 1987.
(10) Munowitz, M. *Coherence and NMR*; Wiley: New York, 1988.

10.1021/ja011088z CCC: $20.00
Published on Web 12/01/2001

experiments, the vibrational spectra can be spread into a number of dimensions so that spatial distributions of couplings and frequencies can be determined. The diagonal part of the 2D-IR spectrum exhibits similar characteristics as would be seen in a linear-IR spectrum. Along the anti-diagonal, however, a narrowed line shape[13] is obtained, thus, providing clarity to a congested IR spectrum. The cross-peaks in a 2D-IR spectrum correspond to the coupling between modes and can be used to determine the three-dimensional structure on the basis of some intermode potential. Although much work remains to be done before such a procedure becomes routine for even the simplest systems, the benefit will be a significant advance in the ability to observe the time evolution of structural changes.[14]

There are extensive experimental measurements in the literature on peptides [5,7,15−19] and more recently on small molecules [19,20] using the 2D-IR method. Figure 1 shows the 2D-IR spectra of one of the dipeptide systems, acetyl proline-NH_2 in chloroform.[15] By comparing the general features of this spectrum with the simulations we intend to illustrate the essential features of 2D-IR spectra and provide a foundation for structural interpretation of 2D-IR. The complex 2D-IR spectrum, $S(-\omega_\tau,\omega_t)$, is obtained in the same manner as NMR−COSY spectra. Two infrared pulses separated by τ generate an FID beginning at $t = 0$ which is measured along the t-axis by heterodyne methods.[15] A double Fourier transform along τ and t yields the spectrum $S(-\omega_\tau,\omega_t)$. The $|S(-\omega_\tau,\omega_t)|$ spectrum is shown in Figure 1a. The three peaks along the diagonal marked B and C correspond to amide-I modes from amino and acetyl ends of the dipeptide, respectively. The diagonal marked A is the amide-II mode from the amino end. The cross-peaks are marked D through I. As shown in ref 15, these cross-peaks are assumed to correspond to two conformations of the dipeptide in chloroform. Cross-peaks H and I are due to coupling between the amide-I modes from the amino and acetyl ends. Others correspond to coupling between the amide-I and -II modes. Figure 1b shows the real part of the spectrum where the peaks are resolved with opposite signs. The splitting is due to anharmonicity. In the case of cross-peaks, the off-diagonal anharmonicity is a measure of coupling between modes. The frequencies positions indicate that the two configurations have almost degenerate amino end amide-I transitions and different amide-II and acetyl end amide-I transitions. Experiments with polarized light substantially improved the spectral discernability of the cross-peaks as shown in Figure 1c. From the relative cross-peaks intensities which change according to differing angular dependencies, it was possible to show that the mean angles between the vibrational transition dipoles that give rise to the cross-peaks H and I are 35 and ∼10, respectively, but the angular distribution was not known.

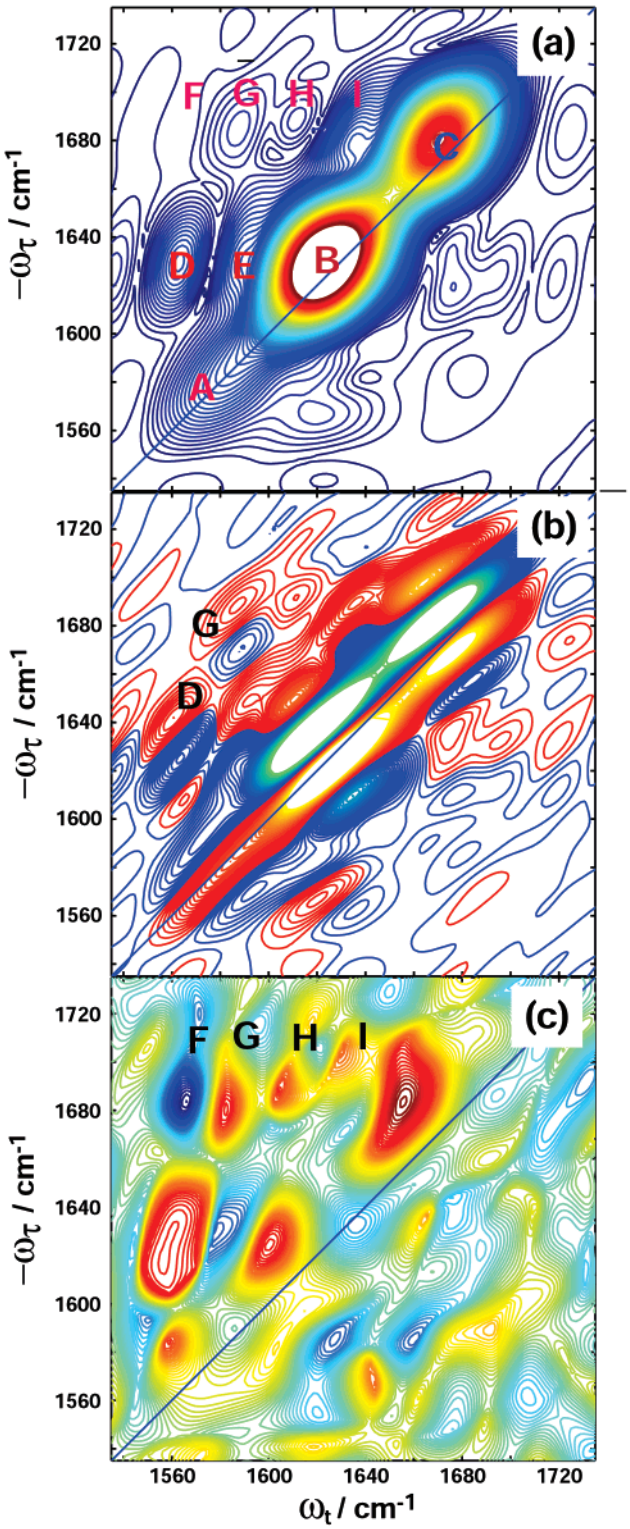

Figure 1. Experimental 2D-IR spectra of acetyl-proline-NH_2 in $CDCl_3$. The magnitude (a) and real part (b) of the complex 2D-IR spectrum, $S\{(-\omega_\tau,\omega_t)\}$, are plotted. The diagonal (A through C) and cross (D through I) are labeled. Increasing 2D-IR signal is represented by color gradient from blue to red. The difference spectrum (c), where the diagonal contributions in the 2D-IR spectrum have been eliminated by subtracting two-polarization measurements, is also shown.

Our main purpose is to provide insight into how the underlying conformational distributions and preferences are manifested in 2D-IR spectra obtained in different solvents. For the simulations we used a simple dipeptide that is terminally blocked by acetyl (Ac-) and methylamide (-NHMe) groups such

(11) Mukamel, S. *Principles of Nonlinear Spectroscopy*; Oxford University Press: New York, 1995.
(12) Zhang, W. M.; Chernyak, V.; Mukamel, S. *J. Chem. Phys.* **1999**, *110*, 5011−5028.
(13) Kubo, R. *Adv. Chem. Phys.* **1969**, *15*, 101.
(14) Hamm, P.; Hochstrasser, R. M. In *Ultrafast Infared and Raman Spectroscopy*; Fayer, M. D., Ed.; Marcel Dekker Inc.: New York, 2001, pp 273−347.
(15) Zanni, M. T.; Gnanakaran, S.; Stenger, J.; Hochstrasser, R. M. *J. Phys. Chem. B* **2001**, *105*, 6520−6535.
(16) Woutersen, S.; Hamm, P. *J. Phys. Chem. B* **2000**, *104*, 11316−11320.
(17) Woutersen, S.; Hamm, P. *J. Chem. Phys.* **2001**, *114*, 2727−2737.
(18) Woutersen, S.; Mu, Y.; Stock, G.; Hamm, P. *Chem. Phys.* **2001**, *266*, 137−147.
(19) Zanni, M. T.; Ge, N.-H.; Kim, Y. S.; Hochstrasser, R. M. *Proc. Natl. Acad. Sci. U.S.A.* **2001**, *98*, 11265−11270.
(20) Golonzka, O.; Khalil, M.; Demirdöven, N.; Tokmakoff, A. *Phys. Rev. Lett.* **2001**, *86*, 2154−2157.

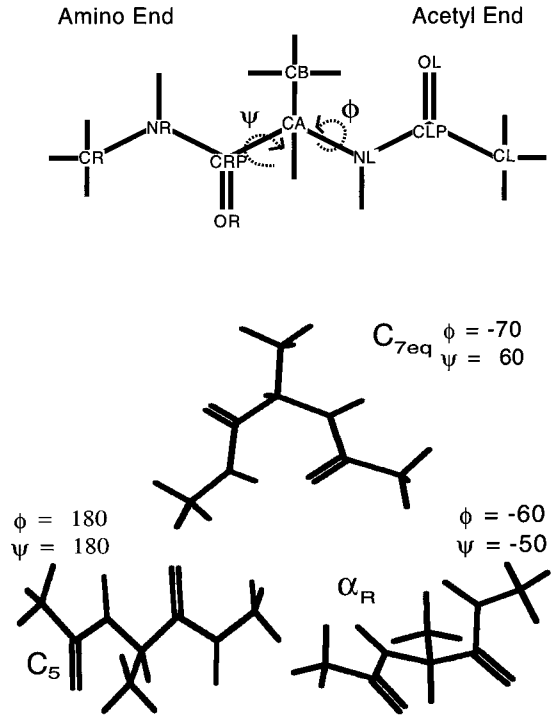

Figure 2. Skeletal diagram of dialanine. The ϕ dihedral angle corresponds to CY−N−CA−C (i.e., rotation about N−CA bond). The ψ dihedral angle corresponds to N−CA−C−NT (i.e., rotation about the CA-C bond). The letter notations of the atoms are taken from the topology file of CHARMM22.[41] Also shown are some of the well-known conformations of dialanine.

that it contains one side chain but two peptide bonds. Dipeptides are biomedically important as protease inhibitors[21] and taste receptors,[22] and for providing receptor selectivity[23] and enzyme regulation,[24] to mention just a few examples. The alanine dipeptide (dialanine) has also served as a paradigm for studying the thermodynamics of protein conformations and folding in different kind of solvents since it is the simplest system to imitate the peptide interaction.[25] It shows features of a polypeptide backbone by having flexible dihedral angles and peptide NH and CO groups capable of hydrogen bonding (H-bonding) with each other or with solvent molecules.

The conformations of dialanine are described in terms of the two dihedral (Ramachandran[26]) angles; ϕ and ψ, defined in Figure 2. Symbols for structures close to the well-known conformations are: the C5 conformer which is the trans/β form of the dialanine; the $C7_{eq}$ and $C7_{ax}$ which are the internally hydrogen-bonded (H-bonded) forms (crystallographic γ and γ'); and α_R and α_L, which are the right-handed and left-handed α-helical forms. The P_{II} form is a polyproline-like conformation. It has been shown experimentally for dialanine that the C7 and C5 forms predominate in nonpolar solvents,[27,28] but that extended forms such as P_{II} and α_R coexist in polar solvents.[28] It has been also shown that as the polarity of the solvent is increased the "signature" of the C7 form diminishes. Theoretical calculations and simulations of dialanine show a similar trend. However, the exact nature of the distribution of extended conformations in polar solvents is not clear.

Since dipeptides are the fundamental building blocks of peptides and proteins, and on account of their small size, they have lent themselves to a wealth of theoretical computations.[25,29] Most of the theoretical work has focused on the relative free energies of the conformers both in a vacuum and aqueous solution. The isolated dialanine has been widely studied by high-level ab intio methods[30,31] and the general conclusion, which was supported by a recent gas-electron diffraction analysis study,[32] is that the internally H-bonded conformation C7eq and extended C5 are of lowest energy. The thermodynamics of conformational equilibria of dialanine in aqueous solution has been investigated using MC,[33] MD,[34−36] and statistical mechanical integral equations.[37] Recent ab initio calculations with the reaction field representation suggested that the aqueous environment stabilizes the helical minima.[38,39] A thorough review has been given by Brooks and Case.[25] These studies agree qualitatively in that the aqueous solvent decreases the free energy differences between conformations and lowers the barriers. Lacking any quantitative experimental evidence, predictions of the relative free energies have been debated. Furthermore, the accuracy and applicability any new methodology or parameters used in dialanine calculations usually have been checked with high level ab initio calculations rather than experimental results. The effects of H-bonding, vibrational excitonic coupling and solvent induced internal coordinate fluctuation have been investigated in the present paper. Two solvents, water (H_2O) and carbon tetrachloride (CCl_4), have been considered. Simulations of the 2D-IR spectrum of dialanine have enabled a quantitative comparison between theory and experiment for the case of dialanine which is expected to be typical for other peptides.

Methodology

The simulations were carried out with the CHARMM program[40] which employed an empirical energy function to represent the external and internal interactions of the system. The classical equation of motion was integrated using Verlet algorithm with a time step of 1fs. The Coulombic and Lennard-Jones nonbonded terms of the potential compensate the H-bonding interactions.[41] Nonbonded interactions were truncated by a group-based force switching function for electrostatic interactions and a regular switching function for van der Waals

(21) Kiso, Y.; Matsumoto, H.; Mizumoto, S.; Kimura, T.; Fujiwara, Y.; Akaji, K. *Biopolymers* **1999**, *51*, 59−68.
(22) Goodman, M.; Zhu, Q.; Kent, D. R.; Amino, Y.; Iacovino, R.; Benedetti, E.; Santini, A. *J. Pept. Sci.* **1997**, *3*, 231−241.
(23) Simone, G. D.; Lombardi, A.; Galdiero, S.; Nastri, F.; Costanzo, L. D.; Gohda, S.; Sano, A.; Yamada, T.; Pavone, V. *Biopolymers* **2000**, *53*, 182−188.
(24) Torreggiani, A.; Tampa, M.; Fini, G. *Biopolymers* **2000**, *57*, 149−159.
(25) Brooks, C. L., III; Case, D. A. *Chem. Rev.* **1993**, *93*, 2487−2502.
(26) Ramachandran, G. N.; Sasisekharan, V. *Adv. Protein Chem.* **1968**, *23*, 283−438.
(27) Cung, M. T.; Marraud, M.; Neel, J. *Ann. Chim.* **1972**, *7*, 183−209.
(28) Madison, V.; Kopple, K. D. *J. Am. Chem. Soc.* **1980**, *102*, 4855.
(29) Schafer, L.; Newton, S. Q.; Jiang, X. In *Molecular Orbital Calculations for Biological Systems*; Sapse, A.-M., Ed.; Oxford University Press: New York, 1998; pp 181−224.
(30) Head-Gordon, T.; Head-Gordon, M.; Frisch, M. J.; C. L. Brooks, I.; Pople, J. A. *J. Am. Chem. Soc.* **1991**, *113*, 5989−5997.
(31) Gould, R. I.; Kollman, P. A. *J. Phys. Chem.* **1992**, *96*, 9255−9258.
(32) Schafer, L.; Bindrees, I. S.; Frey, R. F.; Vanalsenoy, C.; Ewbank, C. *J. Mol. Struct. (THEOCHEM)* **1995**, *338*, 71−82.
(33) Mezei, M.; Mehrotra, P. K.; beveridge, D. L. *J. Am. Chem. Soc.* **1985**, *107*, 2239.
(34) Anderson, A. G.; Hermans, J. *Proteins: Struct., Funct., Genet.* **1988**, *3*, 262−265.
(35) Bolhuis, P. G.; Dellago, C.; Chandler, D. *Proc. Natl. Acad. Sci. U.S.A.* **2000**, *97*, 5877−5882.
(36) Tobias, D. J.; Brooks, C. L., III. *J. Phys. Chem.* **1992**, *96*, 3864−3870.
(37) Pettitt, B. M.; Karplus, M. *Chem. Phys. Lett.* **1985**, *121*, 194.
(38) Gould, I. R.; Cornell, W. D.; Hillier, I. H. *J. Am. Chem. Soc.* **1994**, *116*, 9250−9259.
(39) Shang, H. S.; head-Gordon, T. *J. Am. Chem. Soc.* **1994**, *116*, 1528−1532.
(40) Brooks, B. R.; Bruccoleri, R. E.; Olafson, B. D.; States, D. J.; Swaminathan, S.; Karplus, M. *J. Comput. Chem.* **1983**, *4*, 187.

interactions. In the simulations all of the covalent bond lengths involving hydrogens were constrained using SHAKE. Details of the parametrization, initial setup, minimization, equilibrium, and simulation are given below.

For dialanine, the CHARMM22 parameter set[41] was used. This is an all-atom parameter set. The choice of this parameter set was justified by the reasonable results obtained for the dialanine conformational distribution and vibrational frequencies. The water model used in the simulation is the TIP3P model modified for CHARMM parameters. The TIP3P water model was chosen since with the CHARMM22 parameter set for a protein it leads to a more correct representation of water−peptide interactions. A nonpolarizable Lennard-Jones sphere model was used for CCl_4.[42] Our interest here is to highlight the differences in conformational preference of dialanine between water and a nonpolar solvent represented by this simple model of CCl_4.

The initial pure solvent system consisted of 500 water molecules in a cubic cell with the length of 24.636 Å at 298.15 K. This initial configuration of the solvent box was obtained from earlier simulations of pure solvents. Ab initio calculations showed that dialanine can exist in different conformers.[41,43] So, we have chosen the initial dialanine conformations for solvent simulation from ϕ and ψ values that sample the entire $\phi-\psi$ conformational space. The preferred conformation was obtained by changing the desired dihedrals of dialanine in step-by-step increments of 5° and optimization of the remaining degrees of freedom with Adopted Basis Newton Raphson (ABNR) minimization.

The solute (dialanine) was placed in the center of this periodic box, and the water molecules within 2.1 Å were removed. This resulted in six water molecules being removed. Initially, solvent molecules were minimized with dialanine kept rigid and fixed at the center of box. Eventually, the dialanine was relaxed, and the whole solvated system was minimized. During this minimization procedure, the dihedral angles of dialanine corresponding to various conformers were constrained. However, during the simulations no constraints were applied on these dihedral angles. This solvated system was slowly brought to room temperature and equilibrated for 60 ps. After that the system was allowed to evolve for 100 ps for data collection. Coordinates and velocities of all atoms were saved every 5 fs for analysis. There were a total of 20 simulation sets corresponding to different initial configurations of dialanine. A similar procedure was carried out for dialanine with ∼253 CCl_4 molecules and four simulation sets corresponding to different initial configurations of dialanine were considered.

The amide-I frequencies were calculated by carrying out instantaneous normal mode (INM) analysis for the nuclear configurations of dialanine (excluding surrounding solvent molecules) obtained from the simulation trajectories. The total potential of dialanine was expanded about the initial configuration, and a set of harmonic frequencies was computed. The instantaneous frequency shifts due to H-bonding are included explicitly for the initial configuration. Such a procedure generates an inhomogeneous frequency distribution since it samples all possible initial configurations from an ensemble of nuclear configurations that are in equilibrium at room temperature. Motional narrowing effects are not included. This is a reasonable approach for examining structural distributions since 2D-IR spectroscopy measures the inhomogeneous contributions to the line shapes. The dipole derivatives of different modes of the system are not correctly obtained from the above analysis. We focus only on one mode, amide-I, whose dipole derivative is assumed to be a constant. The INM theory has been successful in describing liquid-state properties,[44] but for our application the term, momentary frequency distribution, may be more appropriate than INM since we are only considering the momentary or instantaneous frequency of a specific internal mode of the solute.

Even though a single normal mode analysis completely neglects both the diagonal and off-diagonal anharmonicities, when this analysis is done for a series of configurations obtained from an MD calculation, some of the anharmonicities are implicitly included since frequencies are calculated from an effective force constant. In these force fields, the intramolecular normal modes are described in terms of internal coordinates such as bonds, angles, and dihedrals governed by the harmonic potential. For small displacements, the linear transformation of these quadratic force constants in internal coordinates into normal coordinates do not cause anharmonicity. At large displacements, however, this linear transformation is not valid and can result in anharmonicity. Additionally, nonbonded interaction potentials, improper angle terms, and barrier crossing of dihedrals will cause anharmonicities. Such terms are reasonable representations of anharmonicities in low-frequency modes, but the extent to which these empirical force fields take into account the coupling between two high-frequency modes is not clear. The amide-I frequencies were identified by the contribution from C═O stretch to that mode. There were no instances where these contributions resulted in crossing (significant mixing) of the adiabatic frequencies, that is, lower and higher amide-I frequencies always came from the motion of same set of atoms. We do not find any occurrence of imaginary frequencies in the amide-I region, suggesting that for the amide-I mode the potential is dominantly a quadratic form with upward curvature in all directions so that the issues related to diffusion and barrier crossing[45] can be neglected. Normal mode analysis was carried out with the VIBRAN module[46] in the CHARMM program.

Results

Calculation of the conformational energy map of an isolated dialanine indicated that in the gas phase, the preferred conformations are either C7 or C5. This is in agreement with earlier calculations using a similar classical force field.[41] In fact, high level ab initio calculations predict a similar trend.[30,31] The interesting question as to what are the most probable conformations in the solvents CCl_4 and H_2O at 298 K is addressed in Figure 3. Two different sets of conformations with very little overlap dominate in each of the solvents. In water, the α_R and P_{II} conformations are most stable, whereas in carbon tetrachloride, the C5 and $C7_{eq}$ conformations are the stable ones.

Normal mode calculations on isolated dialanine indicate that the amide-I frequencies of the acetyl and amino ends are not the same. Table 1 shows the calculated amide-I frequencies for the C5 conformation of dialanine. The amide-I frequency of the acetyl end is about 9 cm^{-1} higher than that of the amino end. This is not surprising since the chemical groups that are bonded to the atoms that mainly participate in the amide-I mode motion at the two ends are different. We have used potential energy distribution (PED) analysis[46] of the amide-I band of dialanine to estimate which internal coordinates of the peptide unit contribute to the amide-I vibrations and to decide whether the amide-I modes are localized on individual peptide units. Table 1 also shows the contribution to the amide-I mode from various internal coordinates. As expected, the main contribution is from the C═O stretch. The mode that gives rise to the higher frequency transition is localized more on the acetyl end of the dipeptide. The lower frequency amide 1 mode arises mainly from the amino end. To separate the overlapping bands, from now on, it is assumed that the carbonyl (C═O) carbon of the amino end is downshifted in frequency by 35 cm^{-1}. This shift is equivalent to that obtained by isotopic substitution by ^{13}C. Normal mode calculations on the isotopomers indicated that isotopic substitution resulted in even more efficient localization of amide-I modes on individual peptide units. We should stress

(41) MacKerell, A. D., Jr.; Bashford, D.; Bellott, M.; Dunbrack, R. L.; Evanseck, J. D.; Field, M. J.; Fischer, S.; Gao, J.; Guo, H.; Ha, S.; Joseph-McCarthy, D.; Kuchnir, L.; Kuczera, K.; Lau, F. T. K.; Mattos, C.; Michnick, S.; Ngo, T.; Nguyen, D. T.; Prodhom, B.; Reiher, W. E., III; Roux, B.; Schlenkrich, M.; Smith, J. C.; Stote, R.; Straub, J.; Watanabe, M.; Wiorkiewicz-Kuczera, J.; Yin, D.; Karplus, M. In *J. Phys. Chem. B* **1998**, *102*, 3586−3616.

(42) Frankland, S. J. V.; Maroncelli, M. *J. Chem. Phys.* **1999**, *110*, 1687−1710.

(43) Smith, P. E. *J. Chem. Phys.* **1999**, *111*, 5568−5579.

(44) Stratt, R. M. *Acc. Chem. Res.* **1995**, *28*, 201−207.

(45) David, E. F.; Stratt, R. M. *J. Chem. Phys.* **1998**, *109*, 1375.

(46) Brooks, B. R.; Janezic, D.; Karplus, M. *J. Comput. Chem.* **1995**, *16*, 1522−1542.

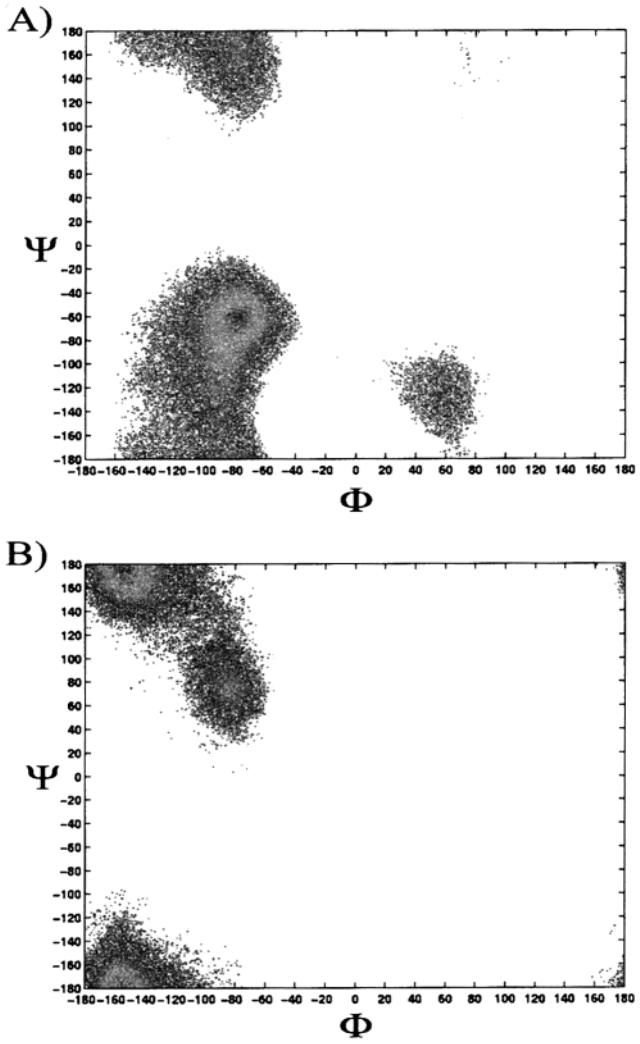

Figure 3. $\phi-\psi$ map of most probable conformers of dialanine in water (A) and CCl_4 (B).

Table 1: Properties of Amide-I Mode of Dialanine[a]

			lower amide-1	higher amide-1
			1676.8 cm^{-1}	1685.6 cm^{-1}
amino end	CRP═OR	stretch	54%	11%
	CRP−NR	stretch	10%	−
	CA-CRP−NR	bend	7%	−
acetyl end	CLP═OL	stretch	11%	56%
	CLP−NL	stretch	−	9%
	CA-CLP−NL	bend	−	6%

[a] Frequencies are listed first. Potential energy distribution for the low and high amide-I frequencies are also given. The internal coordinate contributions to the mode are shown as percentages. Only the contributions greater than 5 % are tabulated. The notations of atoms that participate in the stretching and bending motions are indicated in Figure 2.

that it not our intention to reproduce the amide-I frequency spectrum of dialanine with high accuracy; rather, we aim to provide an approximate and reasonable approach to the amide-I frequency fluctuations and distributions for realistic modeling of 2D-IR spectra.

We now consider the effects of the conformational distributions on the frequencies of the amide-I bands. In general, the amide-I band is influenced by two kinds of interactions: internal vibrational interactions between amide modes and frequency shifts induced by other modes.[2] Other modes could include solvent molecules and the other internal degrees of freedom of dialanine. To take advantage of a nonlinear-IR spectroscopic method, these two interactions should be sensitive enough to be differentiable between conformers. First, consider the strength and distribution of the vibrational coupling which splits the diabatic amide-I bands. The force field used in the simulation does not properly take into account the vibrational frequency dependence on the electrostatic (through-space) potential, $V_{El}(Q)$, between the moving potential charges and charge fluxes. We could add a term:

$$V_{El}(Q) \approx \sum_{k,m} \frac{1}{2}\left[\frac{\partial^2 V_{El}}{\partial Q_k \partial Q_m}\right]_0 \cdot Q_k Q_m \qquad (1)$$

to the force field to incorporate them as done by others.[1,2,47] However, $V_{El}(Q)$ has its most noticeable effect on the amide modes in coupling the nearly degenerate amide-I modes derived from the force field. If the energy gap between the amide-I and other modes of the peptide is large compared with the matrix elements of $V_{El}(Q)$, the relevant effect of $V_{El}(Q)$ can be obtained from a Hamiltonian matrix in the basis of the amide-I modes. The matrix elements of $V_{El}(Q)$ can then be reduced to multipole interactions, approximated by the transition dipole−transition dipole term, β:

$$\beta = \frac{\mu_k \cdot \mu_m - 3(\eta_{km} \cdot \mu_k)(\eta_{km} \cdot \mu_m)}{r_{km}^3} \qquad (2)$$

where μ_k is the vibrational transition dipole vector of the kth amide-I mode, η is the unit vector connecting the indicated dipoles, and r is the distance between dipoles considered large compared with the dynamic charge distribution. The dipole strength was taken as that of *N*-methylacetamide (NMA).[1] The direction and location of the amide-I transition dipole were the same as those used in previous studies of protein amide-I vibrational analysis.[2] Figure 4 shows the dipole−dipole coupling between the amide-I modes of dialanine in H_2O and CCl_4. In water, the coupling distribution is bimodal, one peak centered $\sim$10 cm^{-1} and the other at ~-3 cm^{-1}. However, predominantly a single-peaked coupling distribution centered ~-2 cm^{-1} is observed in CCl_4.

Solvent-induced changes in the nuclear coordinates of dialanine give rise to fluctuations in the amide-I frequencies. Fluctuations arise from direct interaction of the amide-I mode with solvent molecules or through solvent-induced coupling to other modes. Figure 5 shows the distribution of amide-I frequencies due to solvent-induced nuclear fluctuations of dialanine in H_2O and CCl_4. In water, the acetyl end of dialanine gives rise to a broader frequency distribution compared to the amino end. However, in CCl_4 the frequency distribution from the acetyl end fluctuations is narrower than is obtained from those at the amino end.

Another contribution to the amide-I frequency fluctuations arises from the changes in the hydrogen-bond (H-bond) interactions between the C═O and hydrogen donors.[2] Frequency shifts due to such an interaction can be described in terms of geometrical considerations of the solvent molecules or internal atoms which are suitably located to H-bond with C═O. We define an H-bond as existing when the distance between the hydrogen of a donor molecule and the oxygen of the peptide unit is less than the H-bond cutoff distance (2.6 Å) and makes a favorable angle ($\angle$H- -O−X and $\angle$O═C- -X < 90°). A

(47) Lee, S. H.; Krimm, S. *Chem. Phys.* **1998**, *230*, 277−295.

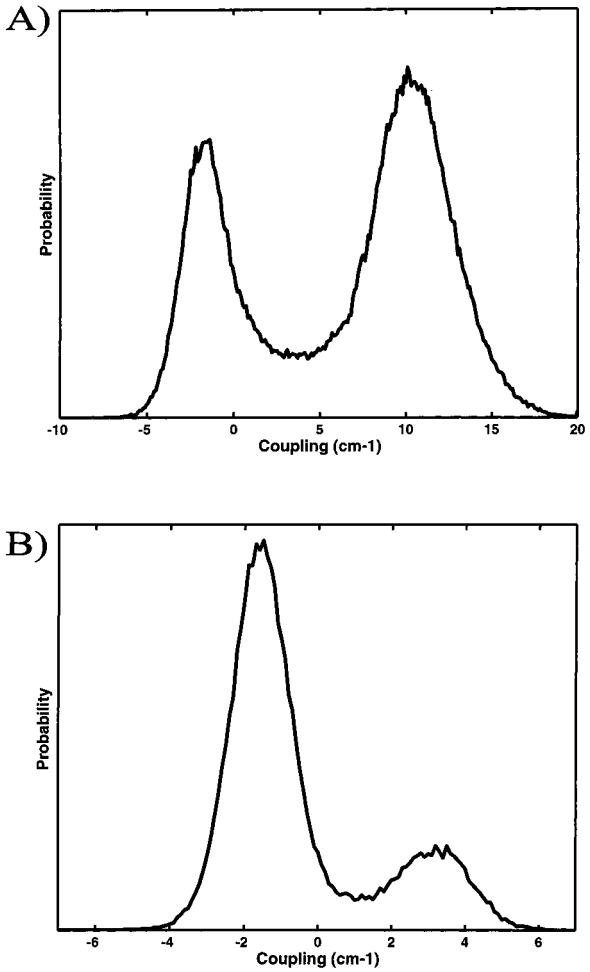

Figure 4. Distribution of coupling between amide-I modes of dialanine due to electrostatic interactions. (A) in H_2O, (B) in CCl_4.

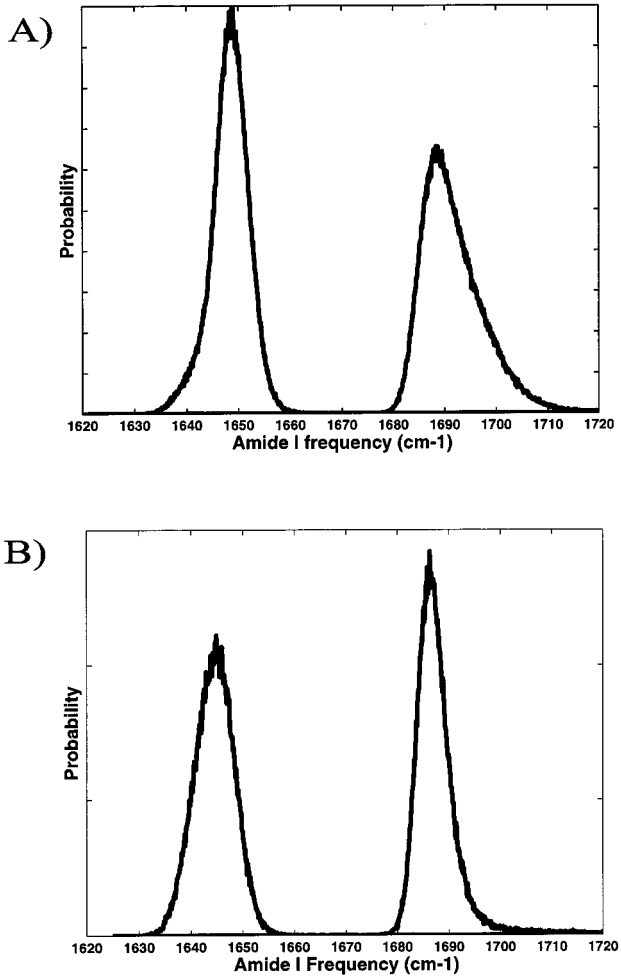

Figure 5. Distribution of amide-I frequencies due to solvent induced nuclear fluctuations of dialanine in H_2O (A) and CCl_4 (B).

pictorial representation of these criteria is shown in Figure 6. When these constraints are satisfied, the shift in frequency $\delta\nu_H$, due to H-bonding is given in cm^{-1} as:[8]

$$\delta\nu_H = 30(r_{OH} - 2.6) \quad (3)$$

where r_{OH} is the C═O- - -H−X distance in Å. In the event that more than one hydrogen atom satisfies the above criteria, the configuration that produces the largest frequency shift is chosen. Figure 7 shows the distribution of frequency shifts due to H-bonding. Analysis of our earlier results on conformational distributions indicated that there are no internally H-bonded structures existing in H_2O. Therefore, the frequency distribution shown in Figure 7A arises solely from H-bonding to water molecules (external H-bonding), arising in ∼95% of the configurations. In CCl_4, however, the only H-bonding is internal. About 20% of the configurations in CCl_4 satisfy the H-bonding geometry criteria. Figure 7B shows the distribution of frequency fluctuations from these configurations. The distribution in CCl_4 is much wider than in H_2O.

In the next section, we discuss possible reasons for the conformational preferences. We will simulate the 2D-IR spectrum and make some predictions as to what one should expect to see in such experiments.

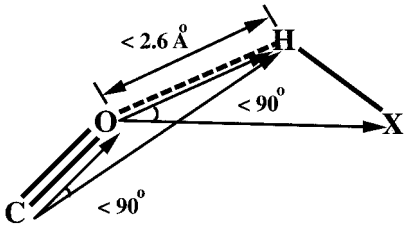

Figure 6. Pictorial representation of H-bonding criteria considered in the calculation. Refer to the text for details.

Discussion

It is well-known that the conformational energy landscape of an isolated dialanine has several minima.. The interest lies in how this conformational energy landscape is affected by different solvents. The conformational distribution dialanine in CCl_4 is similar to what one would expect in the gas phase, namely C5 and C7. The structure where the methyl group is along the equitorial ($C7_{eq}$) is the favored internally H-bonded structure. In H_2O, however, similar conformations do not exist. In fact, conformations similar to right-handed α-helical (α_R) and poly-proline (P_{II}) like structures are observed. The P_{II} form is similar to a twisted β structure, a solvent compromised form. Dialanine conformational distribution at room temperature is consistent with the results from past studies that used similar force field.[41,43]

One aspect of the conformational preferences arises from the competition between the internal and external H-bonding. Conformations can be stabilized by as much as 3 kcal/mol by H-bonding.[14] In H_2O, we find that both external and internal H-bonds can be formed. However, as a result of steric effects

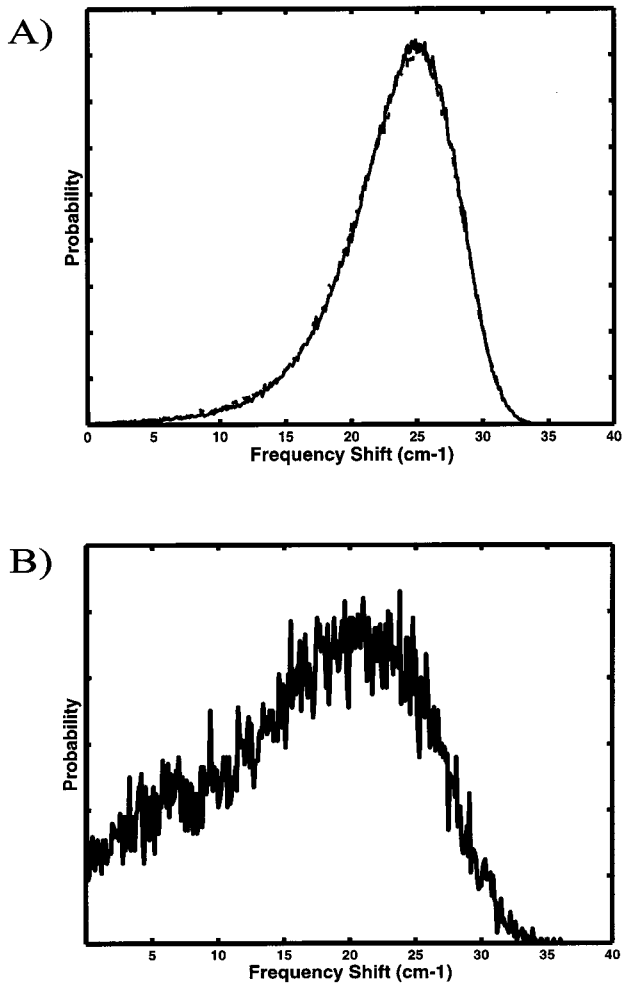

Figure 7. Distribution frequency shifts due to H-bonding. (A) H-bonding of dialanine C═O to hydrogen of water. (B) Internal H-bonding of C═O to H−N of dialanine in CCl_4.

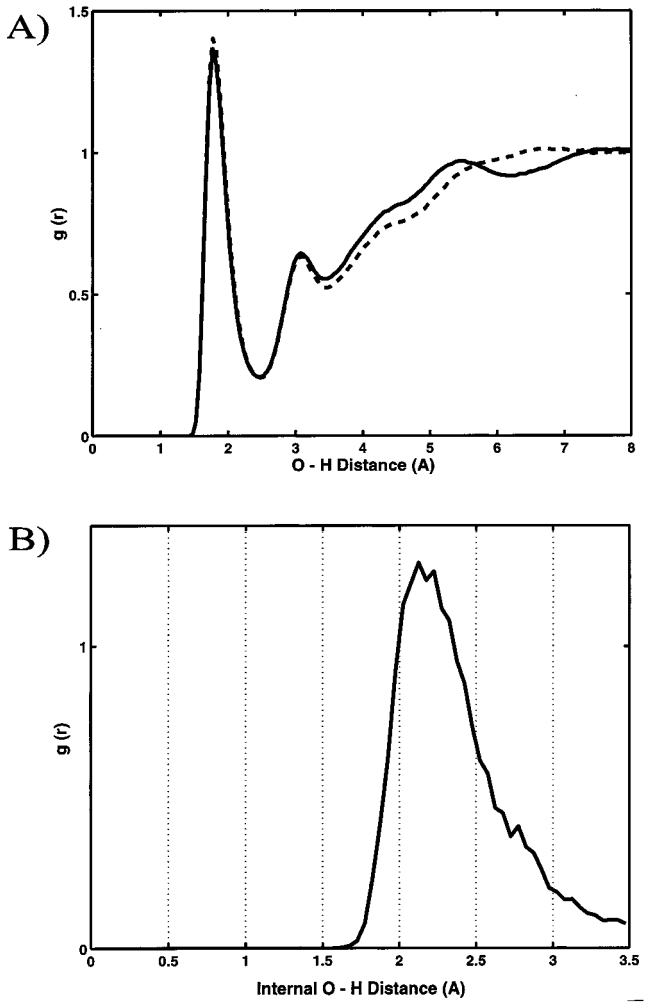

Figure 8. Radial distribution function ($g(r)$) for the externally (A) and internally (B) H-bonded pair. (A) $g(r)$ for dialanine −C═O- - -H− of water (solid line: acetyl end; dashed line: amino end) (B) $g(r)$ of −C═O- - -HN− of dialanine in CCl_4.

and molecular flexibility, the strength and stability of external H-bonding to H_2O is stronger than internal H-bonding. The radial distribution function ($g(r)$) of the O−H of the H-bonded pair for the internally and externally H-bonded cases supports such an argument. Figure 8 shows the $g(r)$ of dialanine in H_2O and CCl_4. It is evident from the figure that the externally H-bonded O- - -H distance is shorter than the internally H-bonded one. Then a distance-dependent potential terms often used in molecular mechanics will predict a strong H-bond energy for the former case. The H-bonding effect on the amide-I frequency shift implicitly suggest such energetics. In water, the external H-bonding of the N−H of the peptide unit to the oxygen of water leads to additional stabilization. Quantum mechanical calculations of the isolated dialanine show that the β (C5) form is still one of the most stable forms. That result is supported by the observation of the C5 form in CCl_4. It is interesting that the externally H-bonded trans form is not found in H_2O. It is suggested that the dialanine prefers a conformation that would produce a large permanent dipole moment, so that it can be solvated well. In fact, the α_R conformer in H_2O does have a large permanent dipole moment.

The electrostatic coupling is determined by the distances between and orientations of the peptide C═O groups which dominate the dipole derivatives. Such a conformational dependence can be seen on the coupling contour map shown as a function of ϕ and ψ dihedral angles (Figure 9). The relevant conformations are marked in the contour map. The α-helical

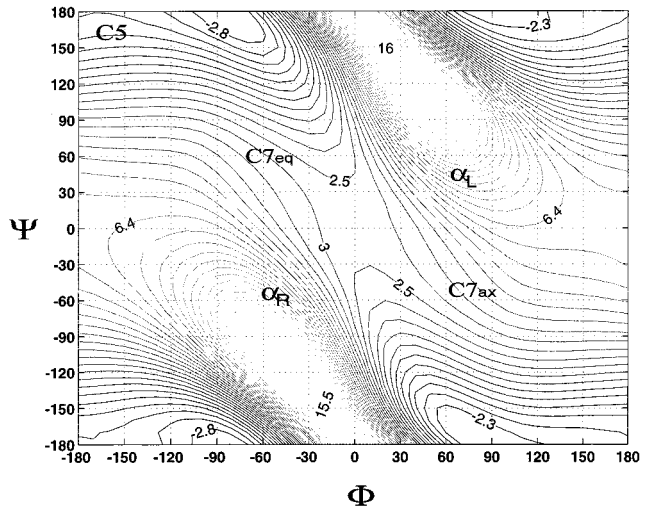

Figure 9. Magnitude of electrostatic coupling between amide-I modes of dialanine as a function of ϕ and ψ dihedral angles. The contour spacing is ∼0.5 cm^{-1}.

conformation, where the transition dipoles are parallel, gives rise to the largest coupling. In contrast, the extended forms C5 and P_{II} that have the C═O bonds closer to a displaced antiparallel geometry also give rise to a small coupling strength.

Furthermore, a perpendicular orientation of dipoles as in the $C7_{eq}$ form, has the smallest electrostatic coupling strength.

Such a distinction in coupling strengths between conformers is evident from the simulation (see Figure 4). In H_2O, there are two very well-separated distributions, a broader distribution at 10 cm^{-1} and a sharp distribution at -3 cm^{-1}, corresponding to the α_R and P_{II} conformations, respectively. In CCl_4, however, there is a strong sharp distribution at low coupling strength, corresponding to C5, and a small peak at a slightly higher strength, corresponding to $C7_{eq}$ conformations. As we have shown below, the distinction between conformations in CCl_4 can be made from the differences in mean amide-I frequencies.

The mean amide-I frequency of each end of the solvated dialanine is determined by whether the C═O from that end forms a H-bond. Since the higher frequency amide-I mode arises from the acetyl end of the peptide, the internal H-bonding in CCl_4 contributes a downshift of 18 cm^{-1} to the higher frequency amide-I band (Figure 7B). Thus, the different conformers in CCl_4 can be isolated in terms of the shift of the acetyl amide-I. In water, almost all conformations of dialanine form external H-bonding. It is evident from Figure 7A, that H-bonds at both ends produce a similar shift, about, 24 cm^{-1}. The first peak in the $g(r)$, which contributes to the frequency shift in our H-bonding model, is identical for both ends. The similarity of the distribution of frequency shift due to H-bonding found at both ends of the molecule supports our earlier reasoning that whatever conformations that are preferred in water maximize the H-bonding to the solvent.

The distribution of frequency fluctuations contributes to the amide-I infrared line shapes.[13] The final amide-I frequency is calculated by subtracting the H-bond frequency shift from the momentary frequency for each dialanine configuration. Figure 10 shows the final frequency distribution for dialanine in H_2O and CCl_4. If the amide-I spectral dynamics can be described in the slow modulation limit, the calculated frequency distribution can be related to IR line shape.[48−52] The slow modulation limit corresponds to the line shape due to the amide-I mode being allowed to vibrate in the static potential created by a fixed configuration of rest of the degrees of freedom, and averaging is done over the fully anharmonic distribution of initial configurations. Any differences in the frequency distribution between the ends in H_2O must arise from the frequency fluctuations caused by the solvent-induced changes in internal coordinates. This conclusion is supported by the results in Figure 9 which indicate that the acetyl end of dialanine gives rise to a larger frequency distribution than the amino end. The results suggest that the amide-I mode atoms from the acetyl end of the molecule have larger displacements from the mean structure since the time-independent INM approach we carried out is a tractable indicator[48,52] of the molecular motions responsible for the generated frequencies. In fact, calculations of the fluctuations of the internal coordinates that participate in the amide-I motion indicate that, specifically, the CA-C−N bending coordinate fluctuations of the two ends are significantly different. One possible reason for the differences in flexibility of the two ends could be that the terminal N−H from the amino end, being more accessible to the solvent, more readily forms H-bonds with the oxygen of H_2O restricting its flexibility.

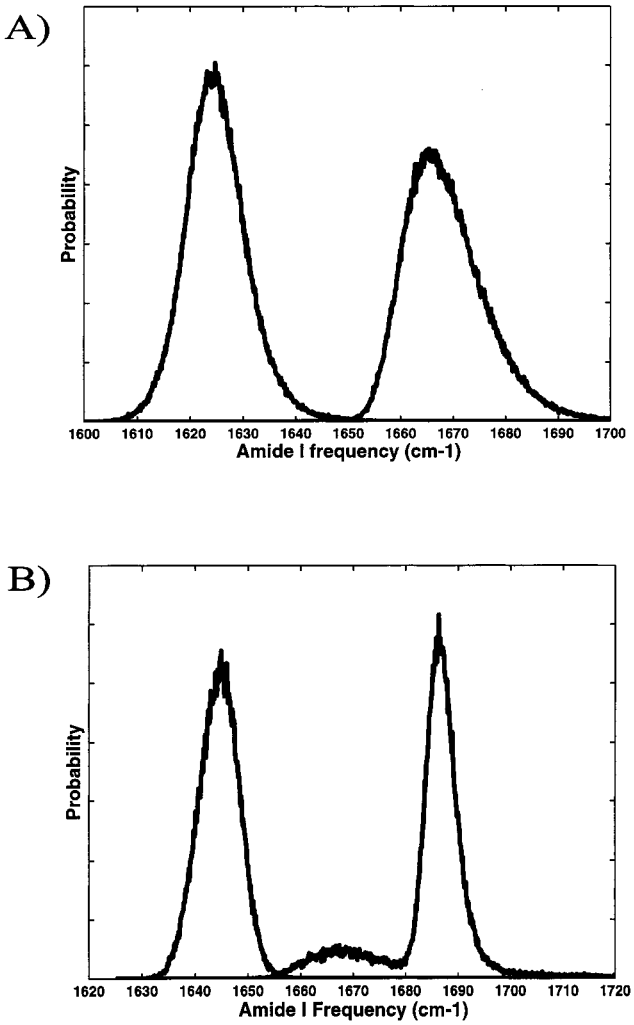

Figure 10. Amide-I frequency distribution for dialanine in H_2O (A) and CCl_4 (B).

One possible reason the acetyl end distribution is narrower than that of the amino end in CCl_4 is that the flexibility of the C═O from the acetyl end is restricted by the tendency to form internal H-bonding. The overall contribution of this $C7_{eq}$ distribution to the amide-I band is about 20%. This differs from the experimentally determined contribution of 70% of the C7 form in CCl_4.[53] The experiments involved a linear-IR study that considered the frequency range between 3200 and 3500 cm^{-1}. One possible reason for the discrepancy is the choice of the force field parameters that are generally developed with the aim of producing an energy minimum at α_R.[29] Table 2 lists some of the characteristics of the amide-I frequency distribution of dialanine in H_2O and CCl_4. Frequency distributions from both ends in H_2O and the amino end in CCl_4 were reasonably represented by Gaussians. The acetyl end distribution in CCl_4 required a sum of two Gaussians. The overall asymmetry of the frequency distribution seen in both CCl_4 and H_2O, which arise from the internal coordinate fluctuations of dialanine is an indication of collisions due mainly to the repulsive part of the Lennard-Jones potential.[42,54] The Gaussian representation may be useful in some applications, but in this paper the simulation results are used explicitly.

(48) Moore, P.; Space, B. *J. Chem. Phys.* **1997**, *107*, 5635−5644.
(49) Ji, X.; Ahlborn, H.; Space, B.; Moore, P. B.; Zhou, Y.; Constantine, S.; Ziegler, L. D. *J. Chem. Phys.* **2000**, *112*, 4186−4192.
(50) Kalbfleisch, T.; Keyes, T. *J. Chem. Phys.* **1998**, *108*, 7375−7383.
(51) Ahlborn, H.; Ji, X.; Space, B.; Moore, P. B. *J. Chem. Phys.* **1999**, *111*, 10622−10632.
(52) Ahlborn, H.; Space, B.; Moore, P. B. *J. Chem. Phys.* **2000**, *112*, 8083−8088.
(53) Neel, J. *Pure Appl. Chem.* **1972**, *31*, 201−225.
(54) Yamaguchi, T. *J. Chem. Phys.* **2000**, *112*, 8530−8533.

Table 2: Characteristics of the Amide-I Frequency Distribution of Dialanine in H_2O and CCl_4[a]

	CCl_4			H_2O		
	$\langle\omega_k\rangle$ (cm^{-1})	σ^2 (cm^{-2})	σ (ps^{-1})	$\langle\omega_k\rangle$ (cm^{-1})	σ^2 (cm^{-2})	σ (ps^{-1})
Internal Coordinates						
amino end	1645	15	0.72	1649	11	0.6
acetyl end	1687	8	0.54	1690	26	1.0
Hydrogen Bonding						
amino end	–	–	–	24	15	0.7
acetyl end	18	75	1.63	24	15	0.7
Total Frequency Distribution						
amino end	1645	15	0.72	1625	30	1.0
acetyl end	1687 (80%)	8	0.53	1667	49	1.3
	1668 (20%)	40	1.19			

[a] Tabulated values are obtained by fitting the distributions to Gaussians. For the definition of acetyl and amino ends, see Figure 2.

Two-Dimensional IR Spectra. The 2D-IR response functions have been discussed elsewhere,[5,6,12,14,15] and so only a summary is given here. We simulate the 2D-IR spectrum that corresponds to the coherent nonlinear spectroscopic method introduced by Asplund et al.[6] and discussed in detail by Mukamel and coworkers.[12] The method involves a sequence of two IR pulses and is analogous to NMR-COSY. For this case, the vibrational response is limited to the $v = 0$, 1, and 2 levels of each oscillator. In the weak coupling limit, where each excitation is predominantly localized on one individual peptide site, the excitation energies depend on the diagonal and mixed mode anharmonicities, Δ_{kk} and Δ_{km} respectively. These anharmonicities can be related to a coupling Hamiltonian by the following simple expressions[7]

$$\Delta_{kk} = \Delta$$

$$\Delta_{km} = 4\Delta\frac{\beta^2}{(\omega_k - \omega_m)^2} \qquad (4)$$

where Δ is the known diagonal anharmonicity of each of the amide-I mode, β the excitation exchange coupling between the two modes, and ω_k and ω_m are the corresponding vibrational frequencies. In this approximation, anharmonicity of the amide-I mode is needed for the nonlinear interaction which eventually produces the 2D-IR signals. There can be other contributions to Δ_{km} from mechanical effects which will not be considered here.

The frequency domain expression used to simulate the 2D-IR spectrum corresponds to the complete photon echo field generated from two vibrators by three IR pulses. The three IR pulses, 1, 2, and 3, incident at time intervals, τ between 1 and 2, and T between 2 and 3, generate a field $E(t; \tau,T)$ for $t \geq 0$.[11] For the case of $T = 0$, the IR field emitted in the direction $-k_1 + k_2 + k_3$ for a system of vibrators involves a number of Feynman paths.[55] The two-dimensional infrared spectrum is obtained from the double Fourier transform of $E(t; \tau,0)$ along τ and t yielding a two-dimensional spectrum map of ω_τ versus ω_t. We consider the 2D-IR spectrum of the particular set of distributions obtained from the simulations. The irreversible relaxation of each component state is introduced through parameters. The expression in the frequency domain for the 2D-IR spectrum then simplifies to

$$\tilde{S}(-\omega_\tau,\omega_t) = \left\langle i\sum_{k=1,2}\left(\frac{1}{i(\omega_\tau + \omega_k) - \gamma_{10}^{(k)}}\right)\left\{\left(\frac{1}{i(\omega_t - \omega_k) - \gamma_{10}^{(k)}}\right) - \left(\frac{1}{i(\omega_t - (\omega_k - \Delta_{kk}) - \gamma_{21}^{(k)}}\right)\right\}\right\rangle + \left\langle i\sum_{k\neq m}\left(\frac{1}{i(\omega_\tau + \omega_k) - \gamma_{10}^{(k)}}\right)\left\{\left(\frac{1}{i(\omega_t - \omega_m) - \gamma_{10}^{(m)}}\right) - \left(\frac{1}{i(\omega_t - (\omega_m - \Delta_{km}) - \gamma_{21}^{(m)}}\right)\right\}\right\rangle \qquad (5)$$

where the inhomogeneous averaging based on the results of the simulation is represented by $\langle....\rangle$. Furthermore, γ_{10} and γ_{21} are the total dephasing rates arising from population decay in the $1-0$ and $2-1$ transitions, respectively. The first term in eq 5 corresponds to the diagonal peaks and the second term to the cross-peaks. The 2D spectrum exhibits resonance peaks at the fundamental frequencies of the exciton states ω_k, and at frequencies $(\omega_k - \Delta_{kk})$ shifted by the diagonal anharmonicity and having opposite phase. In the cross-peak region, pairs of resonance peaks show up (again having opposite sign) which are now separated by the off-diagonal anharmonicity Δ_{km}.

The 2D-IR measurements are based on nonlinear techniques which permit the effects of inhomogeneous distributions to be extracted. The 2D-IR signal from an inhomogeneous distribution of vibrational frequencies representing the range of chemical environments and structures of the amide-I groups was computed from the set of frequencies obtained from the MD simulation. The averaging also incorporated the shifts due H-bonding for each configuration. A fixed, nonfluctuating mean value of $\Delta_{kk} = 16$ cm^{-1}, obtained from experiments[8] on *N*-methylacetamide, was used in the simulations. The off-diagonal anharmonicity, Δ_{km}, was calculated from eq 4 for each configuration of the simulation. The dephasing rates are approximated as, $\gamma_{10} = 1/(2T_1)$ and $\gamma_{21} = 3/(2T_1)$ where T_1 is vibrational population relaxation time for $v = 1\rightarrow0$. We have used a value of $1/T_1 = 1$ ps^{-1} because studies of model compounds, peptides, and proteins have shown that the amide population relaxation is always in this range.[8]

Simulated 2D-IR spectra, Abs $\{S(-\omega_\tau,\omega_t)\}$ and Re $\{S(-\omega_\tau,\omega_t)\}$, shown in Figure 11 illustrate several of the important structural and dynamical findings. Information about the frequency and coupling distributions can be discerned from the 2D-IR spectrum and evaluated. The diagonal peaks have an elliptical shape, with their longest axis in the $\omega_t = \omega_\tau$ direction. The inhomogeneous distribution of a set of correlated transition frequencies shows up only on the diagonal axis of the 2D-IR spectrum ($\omega_t = \omega_\tau$). Perpendicular to this diagonal axis the peaks may show no inhomogeneous broadening (i.e., there is line narrowing) and can be optimally resolved. The experiments show precisely these effects: the diagonal peaks B and C from the experimental spectrum shown in Figure 1a are elongated along the $\omega_t = \omega_\tau$ direction, indicating that there is a distribution of structures fixed on the time scale of the measurement, and the width along the anti-diagonal at the transition frequencies of the amide-I modes is line narrowed.

The contribution of inhomogeneous broadening to the transition of dialanine in CCl_4 and H_2O can be discerned qualitatively by comparing the profiles of the diagonal peaks in Figure 11. Overall, the amide-I frequencies of dialanine exhibit higher inhomogeneity in H_2O than in CCl_4. The profiles of diagonal

(55) Hamm, P.; Lim, M.; DeGrado, W. F.; Hochstrasser, R. M. *J. Chem. Phys.* **2000**, *112*, 1907−1916.

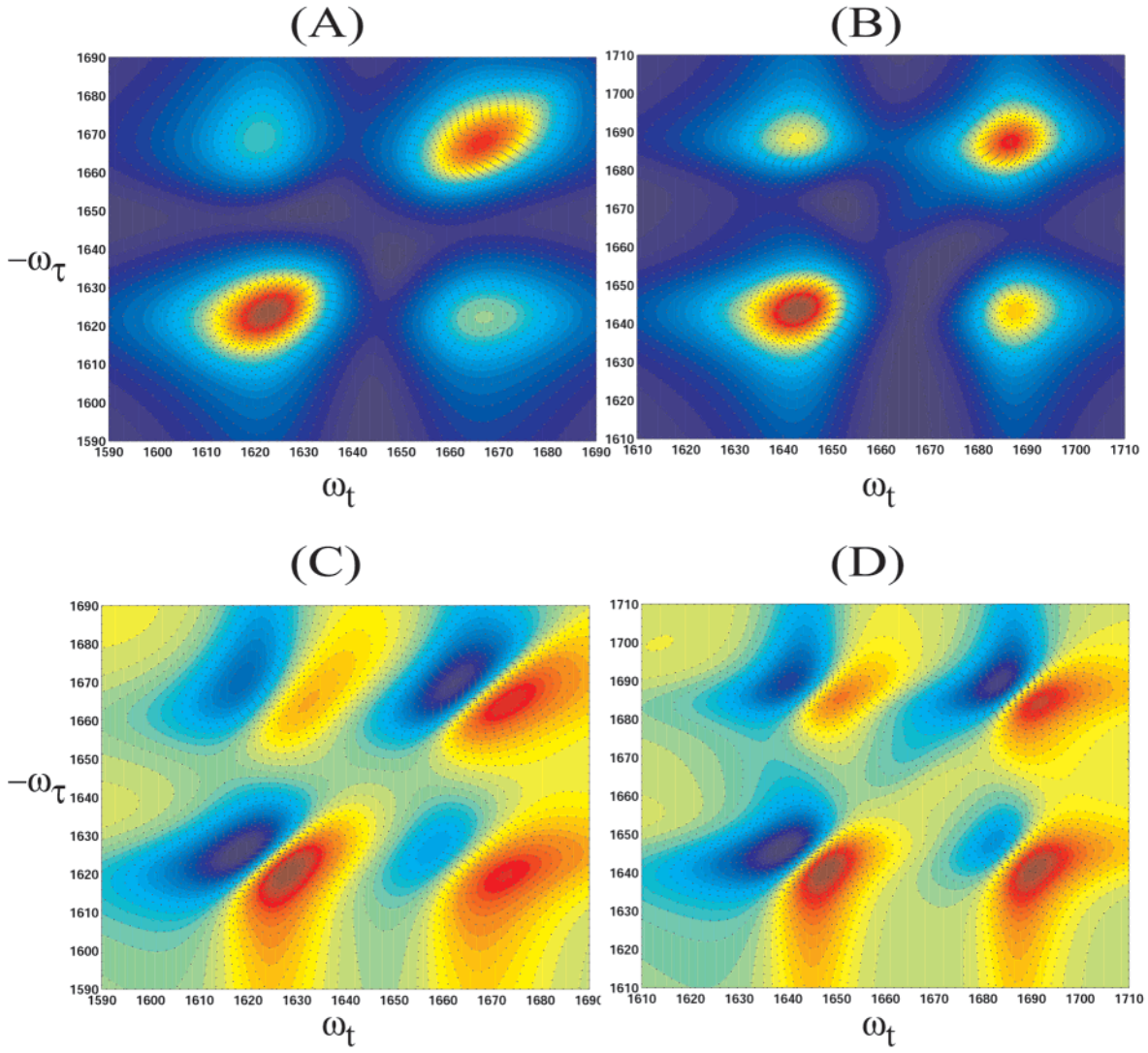

Figure 11. Simulated 2D-IR spectra, Abs$\{S(-\omega_\tau,\omega_t)\}$, of dialanine in H_2O (A) and CCl_4 (B). The real part of $S\{(-\omega_\tau,\omega_t)\}$ also plotted for dialanine in H_2O (C) and CCl_4 (D). Increasing 2D-IR signal, expressed in arbitrary units, is represented by color gradient from blue to red.

peaks in CCl_4 are qualitatively similar with evidence of slight inhomogeneity of the lower frequency diagonal peak. In H_2O, as expected, the higher frequency diagonal peak is much more elongated reflecting the larger inhomogeneous frequency distribution at the acetyl end as calculated earlier. We identified the higher flexibility of acetyl end compared to the amino end of dialanine to be giving rise to a broader structural distribution as a possible reason for the difference in the inhomogeneity between the two amide-I transitions. The results for acetyl-proline-NH_2 dipeptide (Figure 1) show that the inhomogeneous distributions of the two amide-I transitions are different. The simulations suggest different flexibility for the two ends as the explanation for this result.

It is evident from Figure 11, a and b, that the cross-peak region is much more intense for dialanine in CCl_4 than H_2O. This arises because the coupling distribution that gives rise to cross-peaks is wider (or more inhomogeneous) in H_2O. We know from our analysis that the coupling distribution in H_2O is due to multiple conformers. The spectrally integrated cross-peak intensity is the important parameter in determining the magnitude of the coupling, not the apparent intensity of the cross-peak. The experimental spectrum in Figure 1 also shows several cross-peaks that must be indicative of coupling between the modes that are being probed. The simulations suggest that cross-peak between A and B is typical of a strong interaction and a broad distribution.

The nature of different conformers that exist in H_2O and CCl_4 can be discerned from the relative coupling strengths obtained from the real part of the 2D-IR spectrum, Re$\{S(-\omega_\tau,\omega_t)\}$, shown in Figure 11, plots C and D. Each diagonal and cross-peak appears in the 2D spectrum as a pair of a negative (blue) and a positive (red) signals that are separated by the anharmonicities. Although two bands are not seen in Abs $\{S(-\omega_\tau,\omega_t)\}$ the difference in sign of the anharmonically shifted transition allows it to show up in Re$\{S(-\omega_\tau,\omega_t)\}$. Cross-peaks occur at $\{\omega_k, \omega_m\}$ and $\{\omega_k, (\omega_m - \Delta_{km})\}$. Since Δ_{km} is small for dialanine in CCl_4, the cross-peaks with opposite signs are closer to each other in the real part of the 2D-IR spectrum. However, in H_2O, where Δ_{km} is large, there are strong cross-peaks with opposite signs that are well separated. The frequency separation of these cross-peaks is a measure of the coupling, Δ_{km}. So, from the Re$\{S(-\omega_\tau,\omega_t)\}$, the signatures of the large coupling strength conformer, α_R, is apparent in H_2O and those of the low coupling strength conformers, $C7_{eq}$ and C5, are manifested in CCl_4. Furthermore, the extensive cross-peak region signals the presence of the additional conformer, P_{II}, with low coupling strength in H_2O. Figure 1 b shows the real part of the experimental 2D-IR spectrum. We can now see that the cross-peaks D and G

which arise from coupling of mode A with B and C have a large mixed mode anharmonicity, Δ_{km}, compared to those couplings that arise from interaction between modes B and C.

The simulations can help to isolate the transitions that lie underneath the inhomogeneously broadened amide-I band. They indicate that the high-frequency diagonal peak arises from two transitions in CCl_4, but both of them are not apparent in the diagonal peak profile. Since the acetyl end is coupled to the amino end, a pair of cross-peaks occurs for each of the two different acetyl end transitions. So that while the pair of diagonal bands from the acetyl end are not resolved in the diagonal region, they can be discerned in the cross-peak portion of the 2D-IR spectrum. This powerful capability of 2D-IR has been taken advantage of in recent experiments in which the different dependencies of the diagonal and cross-peaks on polarization of the IR fields were utilized to isolate the cross-peak spectrum.[15,19] One such spectrum is shown in Figure 1c where the intensities from the diagonal peaks are greatly diminished. Furthermore, the cross-peak F, not apparent in the Abs $\{S(-\omega_\tau,\omega_t)\}$ shows up clearly for certain polarizations. The simulation confirms that the existence of these multiple cross-peaks arises from overlapping transitions of different conformers hidden within the diagonal peaks.

From the experimental spectrum shown in Figure 1c, it was possible to obtain values for the angles between the vibrational transition dipoles of modes that produce cross-peaks H and I (35 and ~10, respectively). These experiments measure $\langle P_2(\cos\,\theta)\rangle$, where θ is the angle between the vibrational transition dipoles. Each observed value of the ensemble average $\langle P_2(\cos\,\theta)\rangle$ can correspond to two possible angles. From the simulation data, averaging over the whole spectrum, we obtained $\langle P_2(\cos\,\theta)\rangle$ values of 0.27 and 0.09 for dialanine in H_2O and CCl_4, respectively, corresponding in each case to two possible angles between the vibrational transition dipoles. Additional information such as coupling strength and conformational distribution from theory can be used to choose the angle that corresponds to the correct conformer. We have illustrated in Figure 12 how to refine the possible conformations that give rise to a specific cross-peak by relating $\langle P_2(\cos\,\theta)\rangle$ to the Ramachandran angles. Figure 12 A and B show the areas in $\phi-\psi$ conformational space that would give rise to the $\langle P_2(\cos\,\theta)\rangle = 0.27 \pm 0.03$ for H_2O and 0.09 ± 0.03 for CCl_4. Also shown in the plot is the region of the $\phi-\psi$ conformational space which correspond to the calculated coupling of 10 ± 1 cm^{-1} for H_2O and 2 ± 1 cm^{-1} for CCl_4. It is evident from the figure that the right or left-handed alpha helical regions in H_2O, and the C5 and C7 conformational regions in CCl_4 satisfy both constraints. However, only the right-handed α-helical and C7eq are favored over their symmetrical counterparts since the conformational space at room temperature is further restricted by the relative free energies of the conformers. The dashed lines in the plot show the most probable conformational regions as calculated from MD simulations. Since the value of $\langle P_2(\cos\,\theta)\rangle$ is expected to be different at different points on the 2D-IR spectrum, it can be also utilized in isolating conformers that have similar coupling strengths. This kind of refinement process that takes into account the normal-mode analysis, energetics, coupling and $\langle P_2(\cos\,\theta)\rangle$ was considered in providing a qualitative picture of possible conformers in acetyl-proline-NH_2 from the 2D-IR spectra.[15]

The correlation between fluctuations of the different amide-I frequencies can also be evaluated. The frequency distributions obtained from the MD simulation predict the correlation

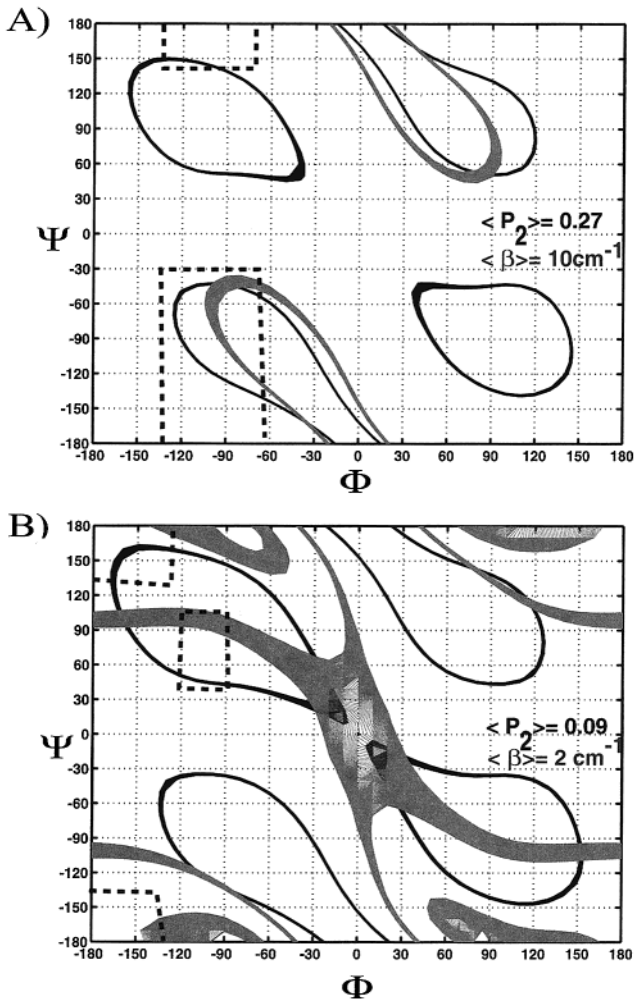

Figure 12. $\phi-\psi$ map of $\langle P_2(\cos\,\theta)\rangle$ and coupling of dialanine in H_2O (A) and CCl_4 (B). The solid dark lines show the $\langle P_2(\cos\,\theta)\rangle$ ±0.03. The solid gray lines show the mean coupling magnitude, $\langle\beta\rangle$ ±1 cm^{-1}. The dashed lines are provided as a visual aid indicating the most probable conformational region (for details refer to Figure 3).

coefficient, ξ, between the distributions for the acetyl (ac) and amino (am) ends amide modes from:

$$\xi = \frac{\langle \delta\omega_{ac}\delta\omega_{am}\rangle}{\sqrt{\langle \delta\omega_{ac}^2\rangle\langle \delta\omega_{am}^2\rangle}} \qquad (6)$$

where, for example, $\delta\omega_{ac} = \omega_{ac} - \langle\omega_{ac}\rangle$ is the deviation of the indicated frequency from the mean. We find $\xi = 0.3$ for dialanine in H_2O. Such a correlation between the amide-I modes is not detectable in a linear-IR spectrum. However, the differences between the 2D-IR spectra in different frequency quadrants, $\text{Abs}\{S(-\omega_\tau,\omega_t)\}$ and $\text{Abs}\{S(+\omega_\tau,\omega_t)\}$, does manifest the effects of correlation between the inhomogeneous frequency distributions.[56] The diagonal peaks that are elongated in the $\text{Abs}\{S(-\omega_\tau,\omega_t)\}$ due to inhomogeneity appear as circular peaks in $\text{Abs}\{S(+\omega_\tau,\omega_t)\}$ if the inhomogeneous distributions of frequencies are not correlated. Figure 13 A shows the $\text{Abs}\{S(+\omega_\tau,\omega_t)\}$ of dialanine in H_2O. The $S(+\omega_\tau,\omega_t)$ signal was simulated using an expression similar to that given in ref 56. Some of the terms leading to the transfer of intensity from the cross-peaks to the diagonal peaks were neglected here. Com-

(56) Ge, N.-H.; Zanni, M. T.; Hochstrasser, R. M. *J. Phys. Chem. A* **2001**. In press.

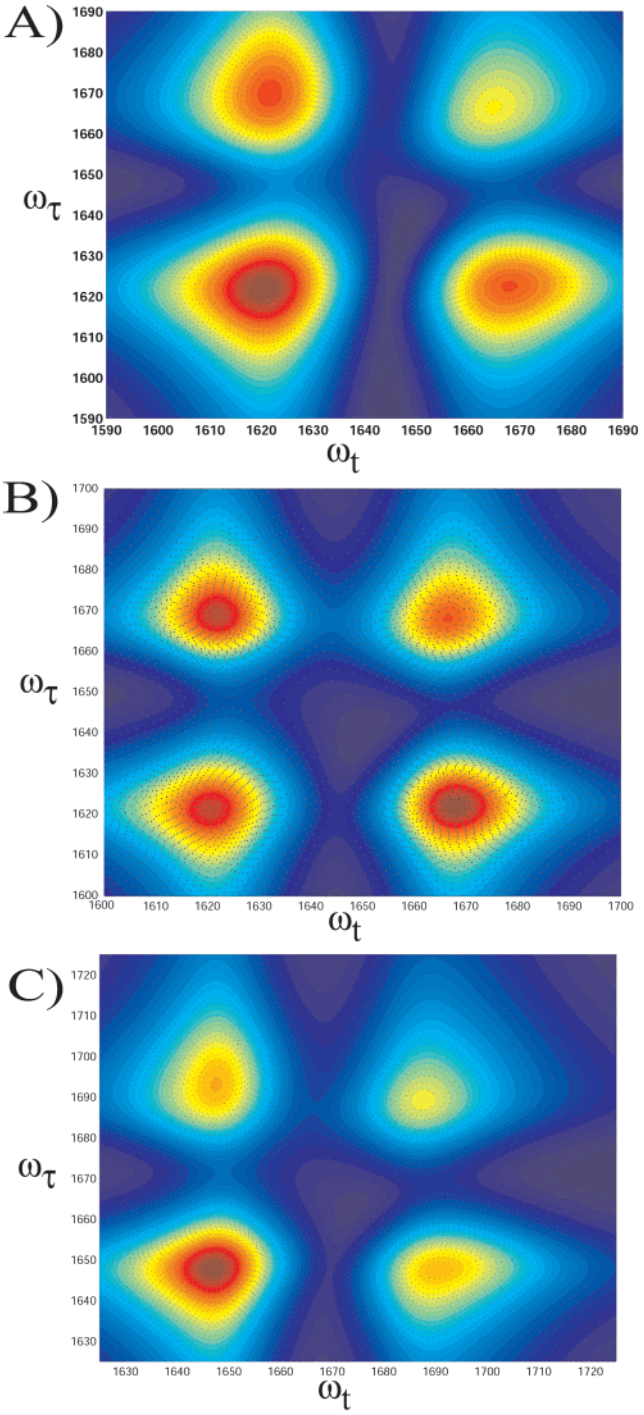

Figure 13. Simulated 2D-IR spectra, Abs$\{S(+\omega_\tau,\omega_t)\}$, of dialanine in H_2O (A). Also shown are the spectra with frequency fluctuations arising only due to H-bonding (B) and internal coordinate fluctuations (C). Increasing 2D-IR signal, expressed in arbitrary units, is represented by color gradient from blue to red.

pared to the Abs$\{S(-\omega_\tau,\omega_t)\}$ spectrum, the diagonal peaks are elongated along the off-diagonal axis. However, the diagonal peaks are not quite circular, evidencing the correlation. The strength of Abs$\{S(+\omega_\tau,\omega_t)\}$ spectrum is also an indication of the width of a distribution. For example, the inhomogeneous frequency distribution from the amino end shows up with an intense diagonal peak and prominent cross-peaks. Very recent experimental measurements which compared the nonrephasing and rephasing 2D-IR spectra of acetyl-proline NH_2 in D_2O[56] have the characteristics illustrated in Figure 13.

The calculations indicate no correlation of the fluctuations from H-bonding at different ends of the molecule in H_2O. More than 80% of the correlation between these two ends arises from the instantaneous normal-mode frequency fluctuations of dialanine. Therefore the correlation between the amide-I frequencies must arise mainly from through bond (mechanical) coupling of the peptide units. We have considered the manifestation of the above two interactions, separately, on the amide-I frequency region of the 2D-IR spectra, $\{S(+\omega_\tau,\omega_t)\}$. Figure 13, B and C, shows the Abs$\{S(+\omega_\tau,\omega_t)\}$ spectra for inhomogeneous amide-I frequency fluctuations arising from H-bonding and internal coordinate motions of dialanine, respectively. As expected, the figure shows near circular diagonal and cross-peaks for the first case and not for the second. In Figure 13B, for the H-bonding case, both diagonal peaks have equal intensities indicating that the frequency fluctuations are statistically independent at both ends of the molecule. Figure 13C shows a difference in intensity between the diagonal peaks indicating that the amino end (lower frequency) has a narrower distribution. The uncorrelated H-bonding case shows intense and circular cross-peaks, whereas the intensity and the circularity are diminished when correlations are included, as evident from Figure 13C. An additional influence of correlation on cross-peaks is that the cross-peaks are displaced more from the diagonal when the fluctuations become more correlated.[56] This example shows how the 2D-IR spectra, $\{S(+\omega_\tau,\omega_t)\}$, can be used to distinguish between correlated and uncorrelated transitions.

Vibrational Energy Transfer Between Peptide Units. We now consider the contribution of energy transfer between the two amide modes of dialanine which is determined by both the fluctuations in the site frequency gap and the coupling between amide-I modes. Fluctuations in coupling can be calculated directly from the solvent induced structure fluctuations which are found to be statistically independent of the frequency fluctuations obtained from the normal mode calculations for each of the structures. The 35 cm^{-1} gap between the amide-I modes validates a localized representation. Therefore, we may use Fermi's golden rule to obtain the energy-transfer rate, $k(\Delta\omega)$, for a given frequency gap $\Delta\omega$,

$$k(\Delta\omega) = \frac{1}{\hbar^2}\int_{-\infty}^{\infty} \langle\beta(0)\beta(t)\rangle\, e^{i\Delta\omega t}\, dt;$$

$$\langle k(\Delta\omega)\rangle = \int_{-\infty}^{\infty} k(\Delta\omega)\Omega(\Delta\omega)d(\Delta\omega) \quad (7)$$

where $\langle\beta(0)\beta(t)\rangle$ is the correlation function of the solvent-induced fluctuations in the electrostatic coupling energy and $\langle k(\Delta\omega)\rangle$ is the average over the frequency gap probability distribution, $\Omega(\Delta\omega)$, which gives the rate of energy transfer in the slow modulation limit. The large frequency gap due to isotopic substitution of the amino end of the molecule shifts $\langle k(\Delta\omega)\rangle$ into the nanosecond regime. These estimates justify excluding the energy transfer between acetyl and amino ends from the calculations of the 2D-IR spectra (i.e., $\langle k(\Delta\omega)\rangle \ll \gamma$).

However, for dialanine that contains two $^{12}C{=}O$ groups, we find the slow modulation limit energy transfer time constants to be shortened to 100 ps and 3 ns in H_2O and CCl_4, respectively. The order of magnitude difference between these rates implies that conformations in CCl_4 experience a low coupling region with a narrow distribution. Thus, the vibrational energy-transfer rate between peptides depends heavily on the nature of conformations that exist in certain solvents. When the H-bond frequency shifts are incorporated into the frequency gap for H_2O, the time constant decreases significantly to 10 ps, indicating the importance of uncorrelated H-bond fluctuations

for vibrational energy transfer. The frequency fluctuations that arise from correlated internal coordinate motions do not influence the energy-transfer rate. Both site frequency fluctuations and site coupling fluctuations will be needed to analyze the vibrational energy-transfer rate when the states are closer and there is fast modulation. For example, the Redfield density matrix formalism can be used in association with the correlation functions obtained from the simulations to compute energy-transfer rates in terms of the spectral densities for the site frequency difference, coupling, and the correlation factors.[57]

Conclusions

From this study we were able to gain insight into the underlying conformational distributions and preferences of solvated dialanine and the way they are manifested in the 2D-IR spectra. Two different sets of dialanine conformations with very little $\phi-\psi$ overlap dominate in the solvents H_2O and CCl_4. In water, the α_R and P_{II} conformations are most stable, whereas in carbon tetrachloride, the C5 and $C7_{eq}$ conformations are the stable ones. Two main factors determine the conformational preferences of dialanine: the competition between intra- and intermolecular H-bonding, and the favorable solvation conditions, that is, conformations with large dipole moment are favored in polar solvents.

We obtained the dependence of the amide-I frequency on H-bonding, vibrational coupling, and solvent-induced internal coordinate fluctuations in two solvents. Normal mode calculations on isolated dialanine indicate that the higher frequency amide-I transition is mainly from the acetyl end of the dipeptide. We have calculated the amide-I frequency distribution for solvated dialanine from the instantaneous normal-mode analysis of the peptide configurations obtained from the simulation trajectories and from the H-bond frequency shifts introduced empirically. The differences in the vibrational frequency distribution of the amide-I band arise from solvent induced fluctuations of the conformers rather than the shifts induced by H-bonding. In water, we find the acetyl end of dialanine to be more flexible than the amino end. The distribution of electrostatic coupling between the amide-I modes calculated from our simulations indicates a clear distinction between conformers. The correlation coefficient for the two amide fluctuations is also distinctly different from unity indicating that the frequency fluctuations at the acetyl end influence those at the amino end.

The simulations provide insight into how the underlying conformational distributions and preferences are manifested in the amide-I region of nonlinear-IR spectra. The 2D-IR spectrum in H_2O shows cross-peaks which are well separated corresponding to a high coupling strength conformer, α_R. The frequency separation of these cross-peaks is a measure of the coupling. It is not apparent either from the linear spectra or from diagonal peak profiles in CCl_4 that there are two amide-I transitions in the high-frequency region. However, they are discerned in the computed cross-peak portion of the 2D-IR spectrum. The profiles of the acetyl and amino end diagonal peaks in CCl_4 are qualitatively similar with evidence of slight inhomogeneity of the lower frequency diagonal peak. In H_2O, as expected, the higher frequency diagonal peak is much more elongated reflecting the broader distribution of structures for the acetyl end. We have also illustrated the nature and origin of the correlation between the frequencies of the acetyl and amino ends of the dialanine. The simulation of the 2D-IR spectrum of dialanine in H_2O also was utilized to show that there is no correlation from H-bonding at different ends of the molecule. The distinction between different relaxation mechanisms will require more complex pulse sequences than those simulated here.

The origins of several 2D-IR experimental signatures were identified. For example: the appearance of cross-peaks due to electrostatic coupling between modes; the elliptical shape of the diagonal peaks due to isolation of homogeneous width from the inhomogeneous width along the anti-diagonal axis; the separation of the diagonal and cross-peaks in the real part of the spectrum due to diagonal and mixed-mode anharmonicities; the existence of multiple cross-peaks due to different conformers and the appearance of more circular diagonal peaks in $S(+\omega_\tau,\omega_t)$ spectra due to uncorrelated inhomogeneous distributions of frequencies. Furthermore, we showed how the 2D-IR spectrum can be interpreted to identify the underlying structural and dynamical information. For example: how to interpret multiple cross-peaks from different conformers; how the differences in the elliptical shape of the diagonal peaks can be related to differences in the structural fluctuations between the modes; how the relative cross-peak intensities can be related to coupling strengths and distributions of different conformers; how the differences between the spectra in different frequency quadrants can be used to identify correlation between frequencies from different parts of the molecule; how to utilize the angular factor along with coupling strength at different points on the polarized 2D-IR spectrum.

Finally, the theoretical interpretation of the 2D-IR spectrum is an evolving process. The CHARMM force field-based molecular dynamics simulations can model 2D-IR spectra without relying on phenomenological parameters. It will be important to compute the vibrational frequency autocorrelation function which decays due to structure fluctuations. Even though classical force field methodology is a reasonable cost-effective way to obtain the frequency shifts it has several drawbacks. The empirical force field being used does not include all the anharmonicity of high frequency intramolecular modes. Only that part that is mediated through other low-frequency modes or through modes that are directly interacting through anharmonic terms or nonbonded interactions is incorporated. It also neglects most of the charge flux influence on the frequencies. We have compensated by incorporating the influence of the vibrational transition dipole interaction between amide-I modes, frequency shifts due to internal and external H-bonding and an experimentally measured value for the amide-I diagonal anharmonicity. To predict dynamics, a more accurate evaluation of the vibrational frequency will be necessary. An ab initio calculation or a specially parametrized empirical potential function might suffice.

Acknowledgment. We thank M. Zanni for useful discussions and for providing the experimental 2D-IR spectra shown in Figure 1 and N.H. Ge for discussions on rephasing/nonrephasing 2D-IR spectra. This research is supported by grants from NSF and NIH.

(57) Gnanakaran, S.; Hochstrasser, R. M. Manuscript in preparation.

JA011088Z